JOURNAL OF MATERIALS SCIENCE 22 (1987) 3547–3555

Defect microstructure and microplasmas in silicon avalanche photodiodes

M. LESNIAK*, D. B. HOLT
Department of Materials, Imperial College of Science and Technology, London SW7 2BP, UK

Soft, noisy silicon avalanche photodiodes were studied using the SEM electron beam induced current technique and transmission electron microscopy. They were found to contain varying concentrations of (i) diffusion-induced misfit dislocations, (ii) precipitates and (iii) cusps (lines of shallower penetration) in ragged p–n^+ junctions due to dislocation-retarded diffusion. The noise was of classical microplasma form but the sites of this breakdown did not correlate with the precipitates as in most previous cases, but occurred at favoured points along the cusps in the p–n^+ junction. Low and intermediate densities of misfit dislocations were found to produce microplasmas with lower breakdown voltages than very high densities. The shallowest misfit dislocations produced the greatest diffusion retardation, suggesting that removal of atoms from the diffusing flux by segregation to the dislocation is the mechanism responsible.

1. Introduction

Silicon reach-through avalanche photodiodes (APDs) are large devices used as photodetectors with GaAs–AlGaAs lasers or light-emitting diodes in the first generation of fibre optic telecommunication links. The absorption coefficient of silicon for infrared light of the wavelength used is relatively low, so the charge-collecting depletion region must be wide to ensure detection of all the incident photons. The devices are operated, therefore, under high reverse bias voltages (350 to 400 V) so the depletion region of the p–n^+ junction widens to "reach through" the whole 150 μm thickness of the slice (Fig. 1). Some gain is desirable so the concentration of acceptors in the lightly doped π material is made such that the field in this region is high enough to produce carrier multiplication by impact ionization. That is, the field accelerates electrons produced by absorbed infrared photons to such high energies that they produce additional electron–hole pairs which are then accelerated and produce others. The result is an "avalanche" of one or two hundred carriers. Electrical noise limits the sensitivity of these devices and can be so severe as to render them useless. Such APDs are known to contain defects [1] and can be spatially electrically non-uniform [2] but no detailed study of the problem has been published as far as is known.

Avalanche breakdown by impact ionization has been studied since 1954 [3] and is understood [4]. Successful devices of the APD type will require high materials perfection and device uniformity because the operating field is near the overall avalanche breakdown value, so any field-concentrating defects are likely to produce premature breakdown. Localized avalanche "microplasma" [4, 5] breakdown in reverse-biased rectifying diodes was early found to correlate with threading dislocations [6]. It was later suggested theoretically [7], demonstrated practically [8] and eventually shown directly by both transmission electron microscopy [9] and SEM electron beam induced current (EBIC) microscopy [10, 11] that the microplasmas in fact occurred at metal-rich precipitates, some of which occurred at dislocations. Combined SEM and TEM studies showed that the precipitates could also form at partial dislocations bounding oxidation- or diffusion-induced stacking faults [12–14]. Dopant impurity precipitates (SiP) with associated local dislocation networks were observed at microplasma sites in shallow, lightly-doped n^+–p junctions in silicon avalanche photodiodes [15]. The $FeSi_2$ precipitates responsible for the electrical degradation of p–n junctions in bipolar transistors, however, acted alone [16]. Resistivity variations lead to localized breakdown in Zener diodes [17] and junction non-uniformities caused by obstructed diffusion (diffusion voids) [17, 18], and cracks or mechanical damage [19] can also be the sites of microplasmas.

At the onset of avalanching, microplasmas switch on and off randomly, producing current pulses of constant height. The microplasma is "on" for an increasing fraction of the time as the voltage increases until it becomes quiescent, i.e. is on steadily. The current carried by the microplasma is limited by heating, spreading resistance and space charge effects. Studies of the dependence of the "off" time on various factors led McIntyre [20] to propose that the breakdown rate P, defined as the reciprocal of the average delay time for avalanching, could be written as

$$P = \tau^{-1} = \gamma P_b \qquad (1)$$

Present Address: BP Research Centre, Chertsey Road, Sudbury on Thames, Middlesex TW16 7LN, UK.

0022–2461/87 $03.00 + .12

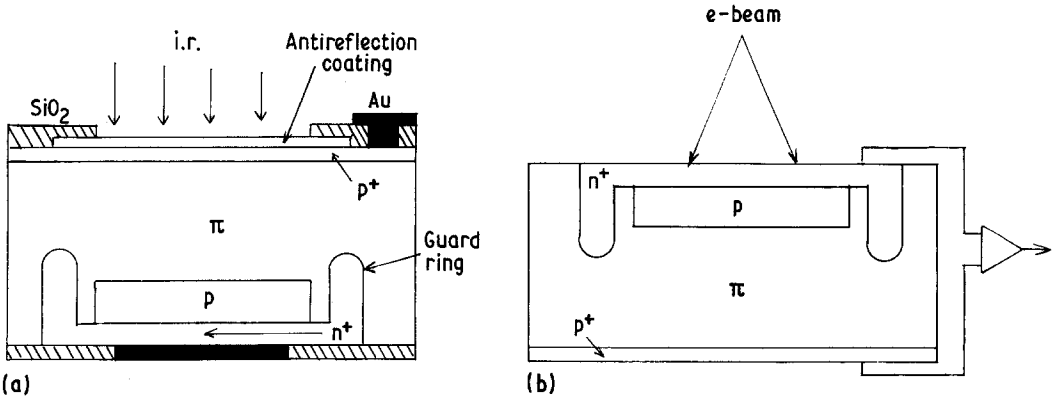

Figure 1 Structure of the silicon reach-through avalanche photodiodes (a) as used to detect infrared radiation and (b) as mounted for SEM EBIC study of the p–n^+ junction region.

where γ is the rate at which triggering carriers arrive in the channel region and P_b is the probability that any one of these actually starts an avalanche. In studies of the electrical characteristics of individual microplasmas [21, 22] the delay or "off" time was defined and measured by means of an expression for the fraction of pulses that have not initiated within t seconds after the application of a small overvoltage pulse which takes the reverse bias from below to above the threshold for avalanching at a particular microplasma site:

$$n_t/n_0 = \exp(-t/\tau) \quad (2)$$

It was shown that τ decreases with increasing overvoltage and is affected by prior pulses which fill traps in the channel, since these can then supply triggering carriers [21, 22].

This paper reports the results of an SEM EBIC study of noisy silicon APDs and reports a new mechanism of microplasma localization at high voltages.

2. Experimental methods

The silicon APDs, kindly supplied by Centronic Ltd (New Addington, Croyden, UK), had the $n^+p\pi p^+$ structure [23] shown in Fig. 1. The diodes were fabricated from π (2×10^{12} cm^{-3}) (1 1 1) silicon. The p layer was formed by implanting a 1.3×10^{13} cm^{-2} dose of 60 keV boron ions followed by a 160 h 1135° C drive-in anneal to give a p layer extending to a depth of 28 μm. The junction was formed at a depth of 8 μm by phosphorus diffusion. Cross-sectional examination by EBIC confirmed that the structure of the devices was as shown in Fig. 1. It was found that the significant defects occurred in the n^+ layer, so the specimens were inverted and remounted as shown in Fig. 1b for the studies reported here.

SEM EBIC studies were carried out on a Jeol JSM-35 microscope. A specially designed charge collection mode detection system was used. This provided low noise, widely-variable-gain amplification with a low input impedance (to give true EBIC, i.e. short-circuit current signals) with back-off, high-voltage bias and signal processing facilities as reported in more detail elsewhere [24].

Specimens were thinned for transmission electron microscope examination in a high voltage (1 MeV) instrument by jet electropolishing followed in some cases by a final ion-beam thinning.

The I–V characteristics of the devices were recorded using a Tektronix Type 576 curve tracer.

3. Results

3.1. Defect microstructure and characteristics

The SEM EBIC signal is the short-circuit current generated by the p–n junction electron voltaic effect. This is closely analogous to the photovoltaic effect on which the device operates, so the high spatial resolution observations are directly relevant. In particular, microplasma sites can be directly observed [15, 17, 19, 25].

Nothing was seen in initial observations on the top, infrared entry faces of the devices, or on cross-sections. Only when noisy devices were inverted so that the n^+–p junction was exposed to the electron beam was defect contrast observed, whereas good devices showed no EBIC contrast in this active, central junction area. The small penetration depth of the electron beam means that the electrically effective defects in the noisy devices were confined to the heavily diffused n^+ layer.

Forty defective APDs were examined on the curve tracer. It was found that the reverse-bias I–V characteristics fell into three groups. About 70% of the devices had a small number of steps in the reverse characteristics, and SEM micrographs showed them to contain a set of well resolved zigzag dark lines representing loci of reduced charge collection due to enhanced carrier recombination as shown in Fig. 2. The network of lines stretched throughout the n^+ region, including the guard-ring area (Fig. 3). Under reverse bias just below the turn-on voltage, a number of current enhancement sites appeared in bright contrast. These are the microplasma sites. (The level of current detected under bias in Fig. 2c is about an order of magnitude higher than in Fig. 2b without bias.) The second group (about 25% of the devices) had nearly ideal reverse characteristics, with a low reverse current up to a sharp breakdown at 400 V in the dark and, when illuminated, a smoothly varying characteristic. However, the avalanche breakdown region was excessively noisy, evidence of which can be seen in Fig. 4a. In SEM EBIC micrographs these APDs were entirely covered by three dense sets of lines at 60° and many ill-defined microplasmas were visible under reverse bias at near breakdown voltages [26]. Fig. 4c was recorded at 312 V and the breakdown value was

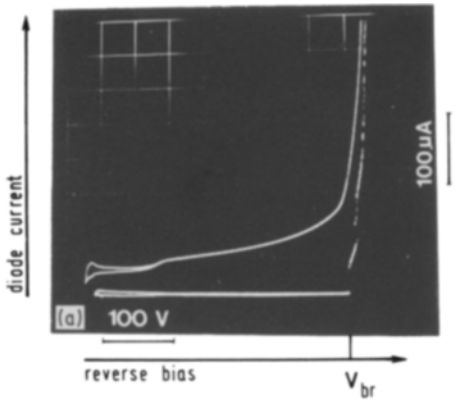

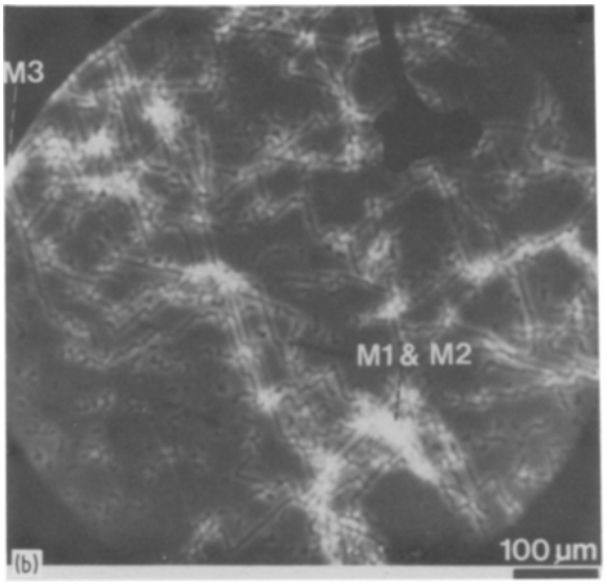

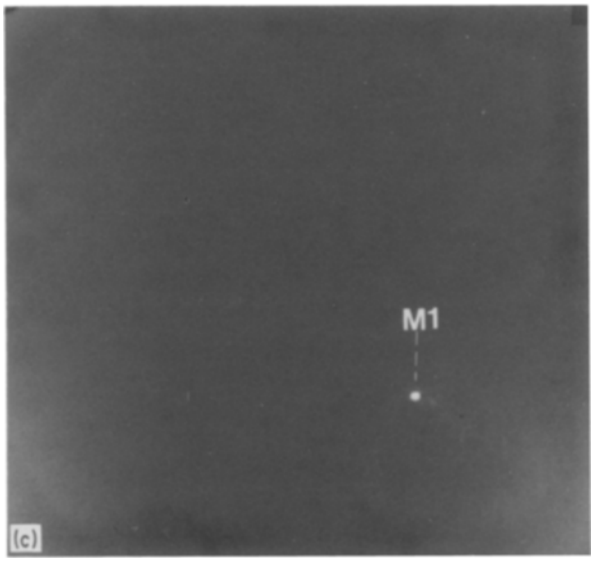

Figure 2 An APD that had (a) a stepped reverse characteristic (the lower curve is I against V in the dark and the upper is under illumination) shown in SEM EBIC micrographs at $T = 77$ K and a reverse bias of 98 V (the breakdown value) for beam voltages (b) 25 keV and (c) 17 keV. In the weak contrast of (c) only the first of the three microplasmas M can be seen.

405 V for this device. A third small group of APDs exhibited greatly reduced breakdown voltages, about 200 V, with a very soft characteristic and typically a single avalanche current discontinuity. SEM microscopy revealed low densities of short, curved lines of varying contrast and, in this specimen, a single large, round microplasma not associated with the dislocation network nodes and believed to be located at a diffusion void (Fig. 5).

3.2. Defect EBIC contrast

The fact that individual dislocations were responsible for the dark line contrast is shown by Fig. 6a which is a montage of TEM micrographs of two dislocations which are also seen in the circled area of the SEM EBIC micrograph in Fig. 6b. A few relatively large precipitates were also seen in some specimens in TEM micrographs [26]. These did not correlate with anything seen in the EBIC pictures and were far too few to account for the microplasmas found in all the APDs. In addition, at shallow depths in the phosphorus-diffused material, numerous small precipitates, presumably of SiP [15], were visible and sometimes dislocations could be seen to be visibly decorated locally (Fig. 7).

In EBIC micrographs at room temperature under reverse biases the dark lines were set in bright stripes (Figs 2b and 5b). In addition very bright spots (microplasmas) appeared under reverse biases near certain threshold, breakdown voltages. These bright spots generally occurred where two or more dark lines ran close together or joined as shown in Fig. 2b. These microplasmas were not always distinct from the bright stripe contrast (Fig. 4c).

The dark lines in most of the APDs were long

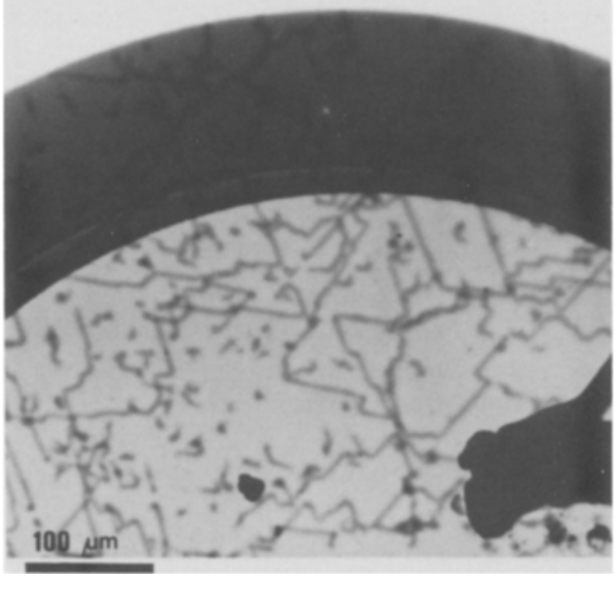

Figure 3 SEM EBIC micrograph of an APD similar to that of Fig. 2 showing misfit dislocations occurring throughout both the lighter junction area and the darker n^+ diffused guard ring. The guard ring is darker because the charge collecting junction is much deeper there (cf. Fig. 1) so fewer carriers survive diffusion to reach it.

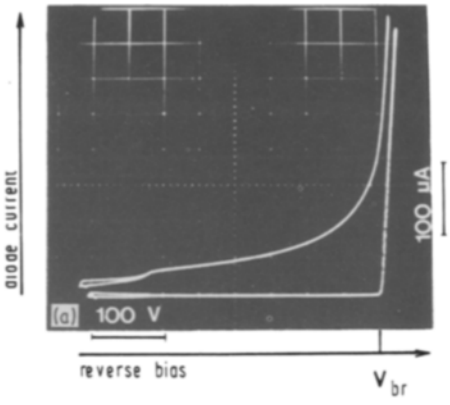

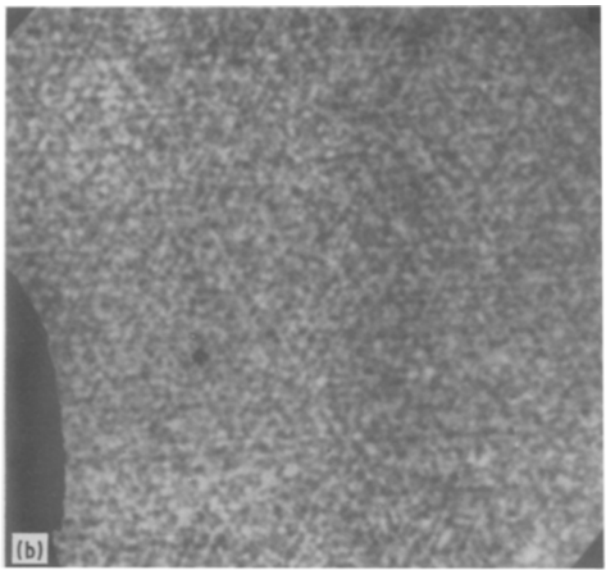

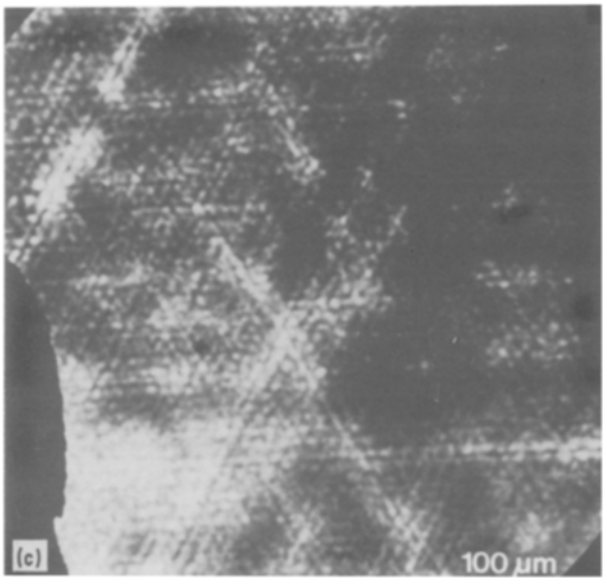

Figure 4 An APD with (a) a hard but noisy reverse characteristic shown in SEM EBIC micrographs taken under reverse biases of (b) 0 V and (c) 400 V.

(fractions of a millimetre in Fig. 2b) so these dislocations ran parallel to the surface. TEM observations showed them to form a planar network. The depth of these (misfit) dislocation networks was established by successively removing the surface layers of the n^+ material until the dark line contrast disappeared in the SEM EBIC micrographs [26]. This was found to coincide with the disappearance of the dislocations in TEM observations on the same specimen, additionally thinned from below. It was established in this way that the misfit dislocations lay at a depth of 2.4 μm. This was confirmed by depth determinations by EBIC linewidth measurements [27]. When the dislocations had been removed the bright stripe contrast was still present [28] so the dislocations were not (directly) reponsible for it. This bright contrast is believed to be due to dislocation-retarded diffusion causing cusps (see Fig. 12 below) in the ragged junction as briefly reported previously [26].

The effect of dislocation depth was studied and it was found that the shallowest dislocations gave the lowest EBIC dark line contrast. The quantitative EBIC dislocation contrast studies that established this will be reported elsewhere. The dislocations again became invisible in the EBIC micrographs at depths greater than about 3 μm. This was not due to the limited penetration range of the electron beams, since the detecting n^+–p junction was at a depth of 8 μm. The apparently short dislocations in Fig. 5 were steeply inclined and continued on down toward the junction. The shallowest dislocations were associated with the greatest bright stripe contrast and with low threshold voltage microplasmas, especially where two or more such dislocations overlapped. This can be seen in Fig. 5, as the dark lines narrow and become fainter in the brightest regions. This visual impression was confirmed by quantitative line-scan observations. The presence of a number of dislocations running up to the surface was responsible for the characteristic large-current, low-voltage microplasma breakdown in APDs of this class.

The dislocations in Fig. 5 are believed to represent an initial stage of formation of the misfit dislocation networks, in which dislocations initially slip into the crystal from the surface. Figs 2 (and 3) and then 4 represent intermediate and final stages of the formation of medium and then high density misfit dislocation networks.

3.3. Microplasma characteristics

The temperature dependence of the breakdown threshold voltage for microplasma noise was measured in the diode of Fig. 2, in which, at the first breakdown voltage, a single microplasma (M_1) was active. The breakdown voltage is that of the "knee" in the I–V characteristic, at which the microplasma began switching a significant current (about 25 μA at the first step in the dark characteristic of Fig. 2a). The breakdown voltage increased linearly with temperature in two ranges as shown in Fig. 8. At liquid nitrogen temperatures the signal to noise ratio of the EBIC current was greatly improved and the threshold voltage reduced, making biasing easier and more stable, so detailed measurements were made at low temperature.

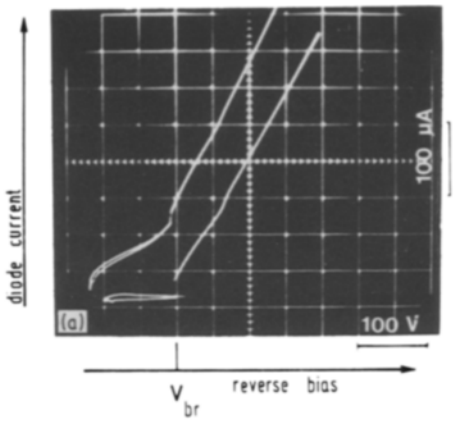

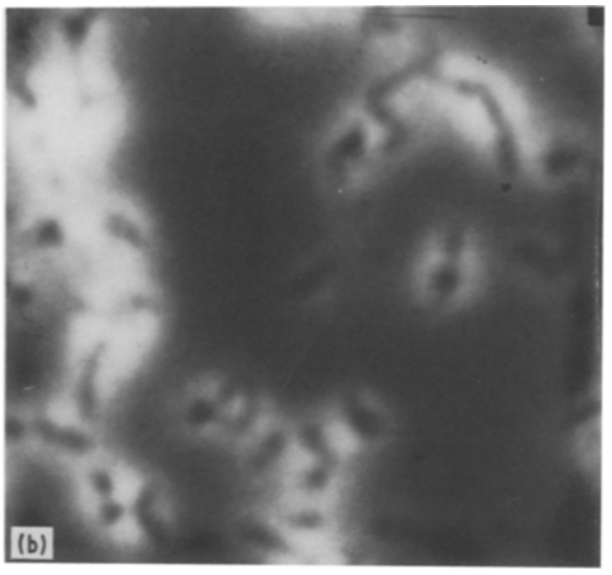

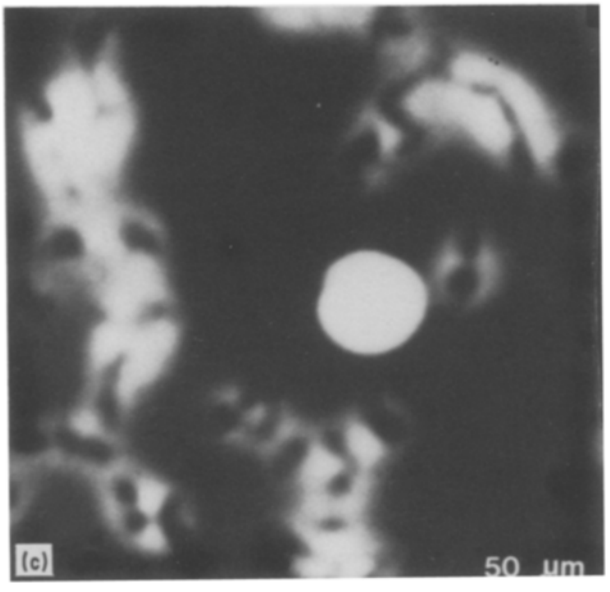

Figure 5 An APD that had (a) a very soft reverse characteristic (lower curve in dark, upper curve under illumination) shown in SEM EBIC micrographs under reverse biases of (b) 50 V and (c) 110 V.

Microplasmas each have a threshold voltage for the onset of avalanching and by a slightly higher voltage are quiescent, i.e. permanently "on". Only between the threshold and quiescent on-voltage do they generate noise or appear distinctly on EBIC micrographs. Only in this voltage range can the incident beam inititate the higher current resulting in a bright spot on the picture. Direct evidence of this relation of EBIC bright spots to soft characteristics and noise is provided by barrier electron voltaic effect short-circuit current line scans. A series of these recorded across microplasma sites at voltages varied through the threshold and quiescent values is shown in Fig. 9. At liquid nitrogen temperature the threshold for microplasma M_1 was 98 V. Consequently the line scan was not noisy at 97.5 V (Fig. 9a) but at 98 V (Fig. 9b) it was very noisy except when the beam was incident on the microplasma site itself, turning the microplasma steadily on. At 100 V, just above the threshold for M_2 (Fig. 9c), the first microplasma was quiescent and not distinguishable among the several peaks of the second site (Fig. 9d). When the beam swept across M_2 in Fig. 9c the whole complex was beam-triggered, giving a smoothly varying current. Elsewhere, however, the trace is then characterized by noise consisting of rapid switching between the upper (on) and lower (off) currents for M_2.

At low temperatures, between the threshold and quiescent breakdown voltages, it was possible to study the electrical characteristics of individual microplasmas. The delay time τ (Equation 2) was measured by applying a voltage pulse and finding the time to the start of the avalanche current pulse. The d.c. bias was held 0.05 V below threshold, and 1.2 V overvoltage pulses were superimposed to switch on microplasma M_1. The fraction of voltage pulses that had not initiated avalanching after a time t fell exponentially in accordance with Equation 2 as shown in Fig. 10, and the data yielded delay time values of 26.8 msec at 83 K and 20.9 msec at 101 K.

Measurements were then carried out using cycles of double overvoltage pulses of the same level. The first pulse was to precondition the microplasma channel by filling the traps and the second to record the breakdown time delays [21]. The time delay to the onset of avalanching after the application of the second pulse, τ_2, was measured as a function of the time lapse between the two pulses, t_p. Following Nield and Leck [21] we write

$$\tau^{-1} + \tau_t^{-1} = \tau_2^{-1} \quad (3)$$

where τ_t is the trap time. The experimental variation of the reciprocal trap time with the pulse separation time given by this relation, shown in Fig. 11, agrees closely with the results of previous workers [21]. (Measurements made over very wide ranges indicated that the obvious interpretation in terms of two trap levels is not correct [22].) This reproduction of the detailed microplasma delay time behaviour reported previously showed that the same trap-activated mechanism operated in the present case, although the junction depth, bias voltage and type of microplasma site in these APDs are very different from those previously studied.

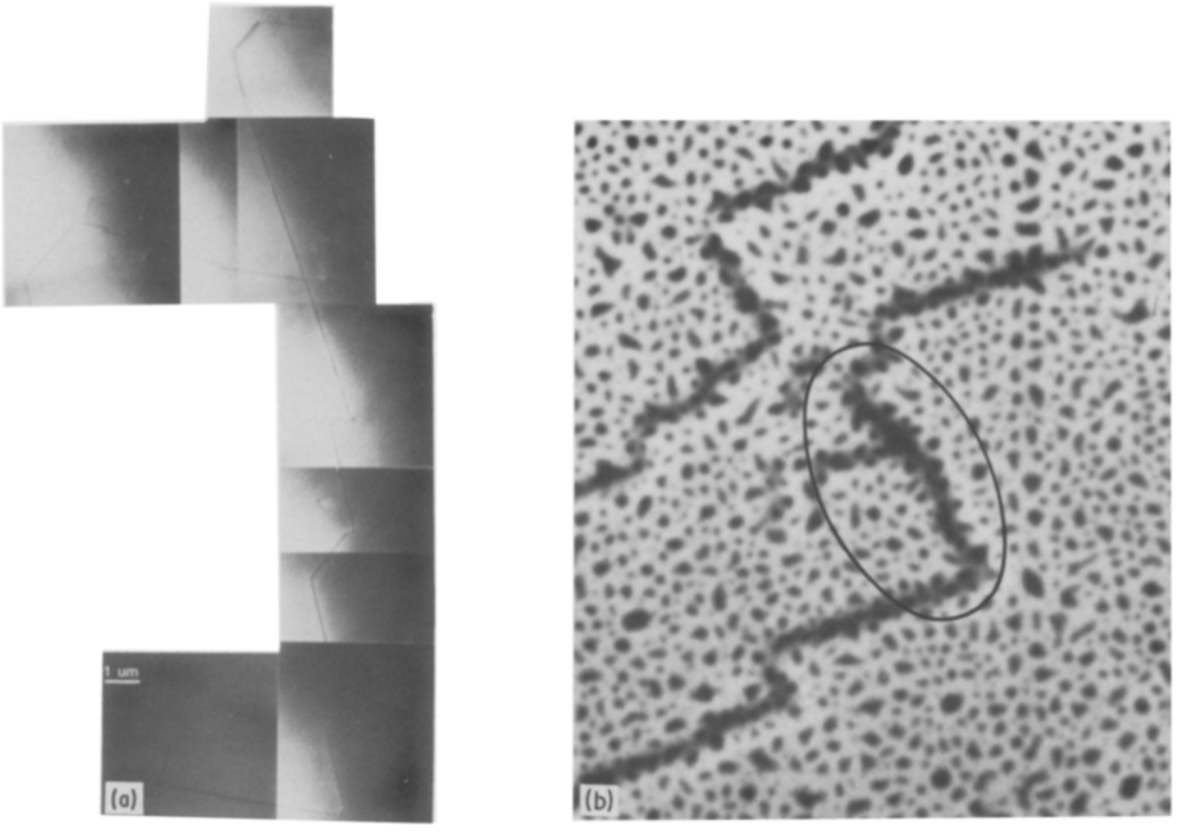

Figure 6 Diffusion-induced misfit dislocations seen in (a) TEM and (b) SEM EBIC micrographs. The (roughly) vertical and horizontal dislocations in (a) corresponded to the dark lines inside the ellipse in (b).

4. Discussion

4.1. Diffusion-induced misfit dislocations

Diffusion-induced dislocations were extensively studied in the 1960s [29–31]. In-diffusion of high concentrations of a dopant with a large atomic misfit, expecially phosphorus and boron, produces lattice parameter variations accompanying gradients in solute concentration which cause internal stress. If this exceeds the yield stress at the high diffusion temperature, plastic slip introduces a network of dislocations. The integrated excess concentration of the dopant required to exceed the yield stress of silicon was calculated by Czaja [29], assuming a complementary error function impurity profile, to be 4×10^{20} cm^3. Experimentally the critical value was found to be about half this. Diffusion-induced dislocations form a network that is essentially planar, parallel to the diffusion front and one to two thirds of the distance of the junction from the surface [31, 32]. The dislocations are of misfit edge type and crystallographically aligned so that in (1 1 1) specimens they form triangular [33] or hexagonal [34, 35] nets ([36] and references therein).

The dark lines in the EBIC micrographs were due to single dislocations (Fig. 6). The evidence that they are diffusion-induced misfit dislocations is as follows:

(i) They occur in and only in the phosphorus-diffused n^+ region (Fig. 3).

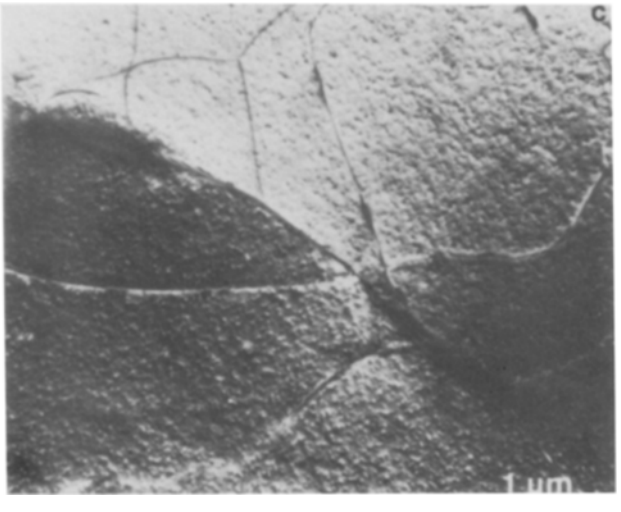

Figure 7 TEM micrograph of an area of a misfit dislocation network showing numerous small dot-like precipitates and evidence of decoration along the dislocation lines.

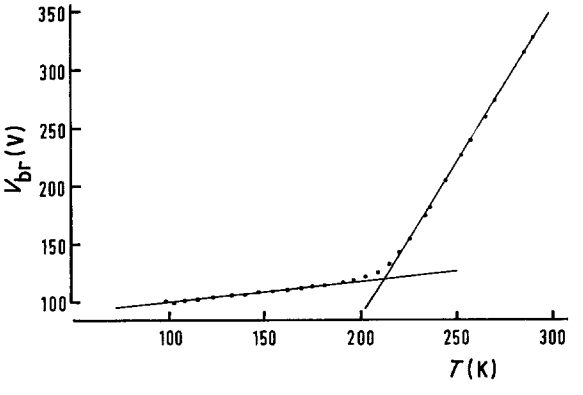

Figure 8 Temperature dependence of the breakdown voltage in the diode shown in Fig. 2.

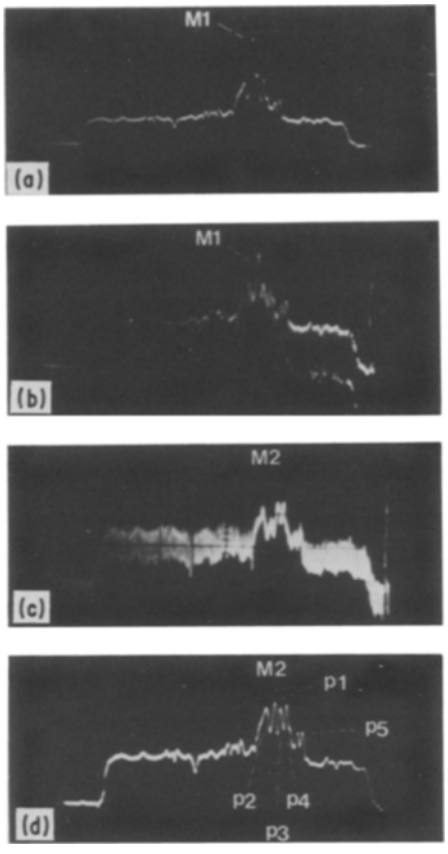

Figure 9 EBIC line scans across microplasmas M_1 and M_2 of the diode of Fig. 2 recorded at $T = 77$ K and reverse biases of (a) 97.5, (b) 98, (c) 100 and (d) 101 V. The thresholds for $M_1$and M_2 were 98 and 100 V, respectively, at this temperature.

(ii) SIMS showed the surface concentrations to vary from about 5×10^{21} to 4×10^{20} cm^{-3}, which is above the critical concentration for inducing misfit dislocations [29].

(iii) The form of the concentration profiles found in APDs that contained dense dark line networks resembled those seen previously in phosphorus-diffused silicon-containing misfit dislocation networks [30] with the phosphorus surface concentration of about 4×10^{20} falling to 2×10^{20} cm^{-3} at the network depth.

(iv) The dark lines formed networks with the alignment and densities previously reported for diffusion-induced misfit dislocations. The cumulative evidence

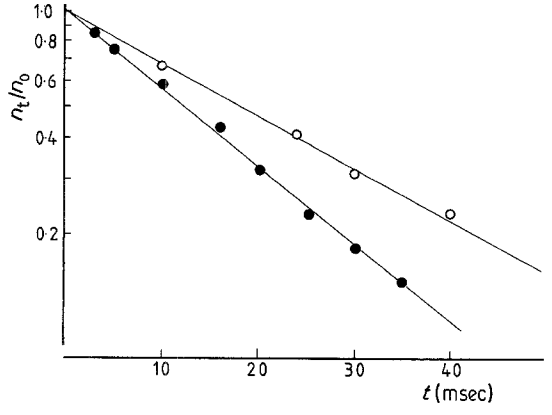

Figure 10 The fraction of overvoltage pulses that had not lead to breakdown in microplasma M_1 (Fig. 2c) after a time t. (●) 101 K, (○) 83 K. Overvoltage 1.040 V.

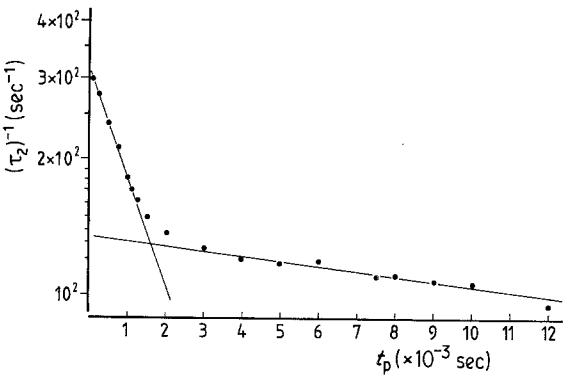

Figure 11 The decay of the contribution to the microplasma decay rate of M_1 due to trap relaxation (Equation 3).

that these are diffusion-induced misfit dislocations is conclusive.

4.2. Dislocation-retarded diffusion

TEM studies carried out in the course of the present investigation showed precipitates to be present at or above the level of the misfit dislocation networks in some APDs [26]. The precipitation of excess phosphorus at concentrations above about 10^{20} cm^3 has been studied in detail [37] and occurs as fine needle-shaped particles elongated along ⟨1 1 0⟩ directions. In the present work the larger precipitates (one or two micrometres long) were too rare (in many specimens there were none) to account for the observed microplasmas. However decoration, i.e. segregation to dislocations, on a scale that was not resolvable by the simple, strong-beam diffraction contrast TEM methods used here, is believed to have occurred at all depths less than 3 μm (Fig. 12). Below 3μm the falling phosphorus concentration results in insufficient impurity decoration to give the strong (about 10%) dark line contrast observed here. Clean dislocations are known to give much weaker EBIC contrast. Segregation to dislocations may also provide the mechanism for dislocation-retarded diffusion.

Dislocation-retarded diffusion is a phrase coined to account for the reduced depth of phosphorus-diffused p–n junctions beneath diffusion-induced slip planes or misfit dislocations. This was first observed by Duffy *et al.* [30] on bevelled and etched sections of phosphorus-diffused silicon transistors. They found that the diffusion of phosphorus is enhanced when its surface concentration is not high and a small number of dislocations is induced, but when a very high concentration of phosphorus like those encountered here, was diffused into silicon and a large number of dislocations was induced then apparently diffusion was retarded below the dislocations. This reduced junction penetration depths locally and produced non-flat "ragged" junctions. Ashburn *et al.* [34] found bright lines in SEM EBIC micrographs of silicon transistors which they attributed to local retardation of the phosphorus diffusion front below the diffusion-induced dislocations.

The zigzag lines in the APD EBIC micrographs recorded under a reverse bias (or at room or elevated temperatures) were seen as dark lines lying in bright stripes [28]. The bright stripe contrast was bias-

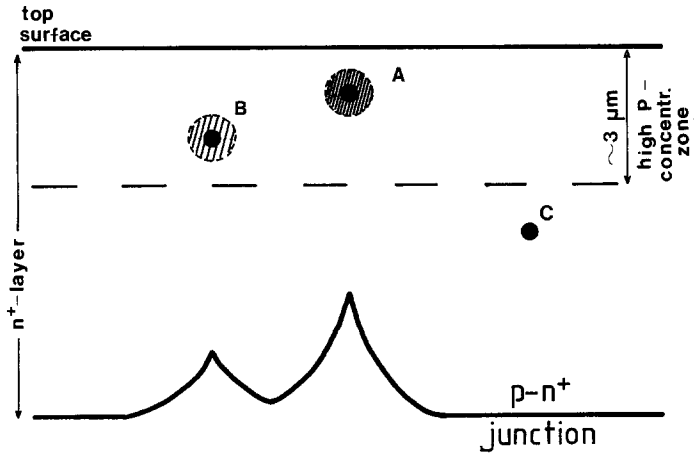

Figure 12 Shallower dislocations like A are more heavily decorated, and by removing more phosphorus atoms from the diffusion flux produce higher dislocation-retarded-diffusion cusps than deeper dislocations like that at B. At depths greater than 3 μm the level of impurity decoration fell too low to give readily detectable dislocation EBIC contrast.

dependent, the dark line contrast was not. Evidence like that of Fig. 6 leaves no doubt that the dark line contrast was due to dislocations. The bright stripes are the loci of sites of enhanced charge collection current. Bright stripe contrast occurred in association with all the misfit dislocations and only in association with them. However, when the material containing the dislocations was removed, the bright stripe contrast remained. This is just what would result from the removal of the superposed dark EBIC contrast lines due to dislocations from the bright contrast stripes arising from locally reduced junction depths below the dislocations, and it is believed that this superposition is indeed the mechanism of the complex contrast observed here. The bright contrast could arise from two effects. The reduced thickness of the n^+ layer means that the holes generated by the electron beam near the top surface have less far to diffuse to reach the charge-collecting junction. Fewer carriers would be lost, by recombination *en route*, at such points. The cusps also act as field concentrators under reverse bias giving an increased long-range charge collecting field locally. However, bright stripe contrast is only seen under large reverse biases, so the field concentration effect must be the important one.

The TEM studies showed that shallow and inclined dislocations were the most heavily decorated. This would be expected since they occur nearest the surface where the phosphorus concentration is highest. By removing from the diffusion flux the largest numbers of phosphorus atoms such dislocations would most retard the diffusion front below, producing the highest cusps as shown in Fig. 12. Similarly where several dislocations of the misfit network meet in a node or run close together, the combined effect will be to remove increased numbers of atoms from the diffusion flux and again produce a higher than average cusp. These highest cusps would be sites of the greatest field concentration and so would undergo breakdown first. Microplasmas were found at just such points.

4.3. Microplasma sites

All previous studies of microplasmas have been carried out on shallow (less than 1 or 2 μm) junction, low-voltage devices. Microplasmas have been found to arise at (e.g.) cracks [19], some but not all threading dislocations [6] and especially at metal-rich precipitates [9]. Evidently, microplasmas are most often found at sites that act as nucleation centres for impurities. Dislocations and stacking faults that are not decorated seem never to generate high-field effects [33, 34]. In addition it has been shown that resistivity variations, e.g. at striations [17], and junction non-uniformities (diffusion "voids"), due to inadvertent masking of a portion of the area by residual oxide caps [17, 18], cause microplasmas.

The microplasma sites in this study were identified as parts of bright stripes with the strongest current enhancement effects (e.g. Fig. 9). The contrast of microplasmas and bright stripes was very similar: the reverse-bias voltage dependence, the lack of any sharp outlines to the bright areas and the general occurrence of microplasmas along stripes (Fig. 4) is striking. The unusual microplasma in Fig. 5 appears similar to diffusion void sites [17, 18] and electrically like the other microplasmas seen in these APDs. This strongly suggests that the microplasma sites were unusually high or sharply curved cusps due to dislocation-retarded diffusion. The evidence that shallow or intersecting dislocations produce the highest cusps is strong.

This enables us to understand the occurrence of three types of *I–V* characteristic in the soft, noisy APDs. There are several distinguishable stages in the formation of diffusion-induced misfit dislocations. First the stresses generate dislocations at the surface which begin to run down into the material (Figs 5b and c). These dislocations, being very shallow, absorb many phosphorus atoms and produce a few very high cusps. The result is a few microplasmas with very low breakdown voltages. Consequently the reverse *I–V* characteristic is very soft and exhibits a few well separated steps, each due to a single large microplasma (Fig. 5a). The second stage involves the dislocations propagating down to the correct depth and interacting to begin forming part of an incomplete misfit dislocation network (Figs 2b and c and Fig. 3). Microplasmas arise both at nodes of the incipient network and at points where the original dislocations loop up to the surface. The microplasmas are more numerous but have higher breakdown voltages. The characteristic is still soft, but begins to exhibit noise and more numerous breakdown steps due to microplasmas above a much higher threshold voltage (Fig. 2a). Finally there results a complete misfit dislocation network with too fine a spacing to be resolved in the SEM

(Figs 4b and c) and diffusion is almost uniformly retarded everywhere. The characteristic exhibits breakdown first at a voltage very near that for homogeneous avalanche breakdown of a perfect device and appears hard. However there is severe noise at breakdown due to the very large number of microplasma-site cusps with approximately the same breakdown voltage.

4.4. Device noise

Fig. 9 and the correlation just discussed leave no doubt that microplasmas caused the soft characteristics and noise in these devices. The presence of any microplasma noise means that the APD cannot provide the desired high gains, i.e. it cannot be operated under a reverse bias very near the homogeneous breakdown voltage. The evidence is strong that microplasmas are due to initiation of breakdown in the usual way [19–21] at the highest cusps in the n^+–p junction. It can be concluded that all the observed defects (misfit dislocations, precipitates, bright EBIC stripes and microplasmas) were consequences of excessively high initial dopant concentrations. These lead to both precipitation and the formation of diffusion-induced misfit dislocations. The latter in turn caused dislocation-retarded diffusion and consequent "ragged" junctions and microplasmas. These, finally, produced electrical noise which is the symptom resulting in device rejection.

References

1. L. J. M. BOLLEN, J. J. GOEDBLOED and E. T. J. M. SMEETS, *Philips Tech. Rev.* **36** (1976) 205.
2. L. J. MAYES, *Electro-optic System Design* (December 1982) p. 28.
3. K. G. McKAY, *Phys. Rev.* **94** (1954) 877.
4. H. KRESSEL, *RCA Rev.* **28** (1967) 175.
5. D. J. ROSE, *Phys. Rev.* **105** (1957) 413.
6. A. G. CHYNOWETH and G. L. PEARSON, *J. Appl. Phys.* **29** (1958) 1103.
7. W. SHOCKLEY, *Solid State Electron.* **19** (1961) 35.
8. A. GOETZBERGER and W. SHOCKLEY, *J. Appl. Phys.* **31** (1960) 1821.
9. A. G. CULLIS and L. E. KATZ, *Phil. Mag.* **30** (1974) 1419.
10. K. V. RAVI, C. J. VARKER and C. E. VOLK, *J. Electrochem. Soc.* **120** (1973) 533.
11. C. J. VARKER and K. V. RAVI, *J. Appl. Phys.* **45** (1974) 272.
12. K. V. RAVI, C. J. VARKER and C. E. VOLK, *J. Electrochem. Soc.* **120** (1973) 533.
13. C. J. VARKER and K. V. RAVI, *J. Appl. Phys.* **45** (1974) 272.
14. J. HEYDENREICH, H. BLUMTRITT, R. GLEICHMANN and H. JOHANSEN, *J. Physique* **40** Colloque (Supplement) **C6** (1981) C6-23.
15. C. DONOLATO, P. G. MERLI and J. VECCHI, *J. Electrochem. Soc.* **124** (1977) 473.
16. P. D. AUGUSTUS, J. KNIGHT and L. W. KENNEDY, *J. Microsc.* **118** (1980) 315.
17. C. J. VARKER, in Proceedings of 9th Annual Conference on Reliability Physics (IEEE. New York, 1971) p. 155.
18. J. W. GAYLORD, *J. Electrochem. Soc.* **113** (1966) 753.
19. N. F. B. NEVE, K. A. HUGHES and P. R. THORNTON, *J. Appl. Phys.* **37** (1966) 1704.
20. R. J. McINTYRE, *ibid.* **32** (1961) 983.
21. M. W. NIELD and J. M. LECK, *ibid.* **18** (1967) 185.
22. K. I. NUTALL and M. W. NIELD, *Solid State Electron.* **18** (1975) 13.
23. T. KANEDA, H. MATSUMOTO and T. TAMAOKA, *J. Appl. Phys.* **47** (1976) 3135.
24. M. LESNIAK, B. A. UNVALA and D. B. HOLT, *J. Microsc.* **135** (1984) 255.
25. D. FATHY, T. G. SPARROW and U. VALDRE, *ibid.* **118** (1980) 263.
26. M. LESNIAK and D. B. HOLT, in "Microscopy of Semiconducting Materials", Conference Series No. 67, edited by A. G. Cullis, S. M. Davidson and G. R. Booker (Institute of Physics, Bristol, 1983) p. 439.
27. D. B. HOLT and M. LESNIAK, *Izv. Acad. Nauk SSSR* to be published.
28. M. LESNIAK, E. NAPCHAN and D. B. HOLT, in "Electron Microscopy and Analysis", Conference Series No. 68 (Institute of Physics, Bristol, 1983) p. 119.
29. W. CZAJA, *J. Appl. Phys.* **37** (1966) 3441.
30. M. C. DUFFY, F. BARSON, J. M. FAIRCHILD and G. H. SCHWUTTKE, *J. Electrochem. Soc.* **115** (1968) 84.
31. E. LEVINE, J. WASHBURN and G. THOMAS, *J. Appl. Phys.* **38** (1967) 81.
32. *Idem, ibid.* **38** (1967) 87.
33. C. GHEZZHI and J. SERVIDORI, *J. Mater. Sci.* **9** (1974) 1797.
34. P. ASHBURN and C. BULL, *Solid State Electron.* **22** (1979) 105.
35. K. V. RAVI, "Imperfections and Impurities in Semiconductor Silicon" (Wiley, New York, 1981) p. 137.
36. D. B. HOLT, *J. Phys. Chem. Solids* **27** (1966) 1053.
37. M. SERVIDORI and A. ARMIGLIATO, *J. Mater. Sci.* **10** (1975) 306.

Received 19 September
and accepted 8 December 1986